In Situ Fabrication Of Quasi-Free-Standing Epitaxial Graphene Nanoflakes On Gold

Philipp Leicht,[†] Lukas Zielke,[†] Samuel Bouvron,[†] Riko Moroni,[†] Elena Voloshina,[‡] Lukas Hammerschmidt,[§] Yuriy S. Dedkov,[⊥,∥] and Mikhail Fonin[†,*]

[†]Fachbereich Physik, Universität Konstanz, 78457 Konstanz, Germany, [‡]Institut für Chemie, Humboldt Universität zu Berlin, 12489 Berlin, Germany, [§]Institut für Chemie und Biochemie, Freie Universität Berlin, 14195 Berlin, Germany, and [⊥]Fritz-Haber-Institut der Max-Planck-Gesellschaft, 14195 Berlin, Germany. [∥]Present address: SPECS Surface Nano Analysis GmbH, Voltastraße 5, 13355 Berlin, Germany.

ABSTRACT Addressing the multitude of electronic phenomena theoretically predicted for confined graphene structures requires appropriate *in situ* fabrication procedures yielding graphene nanoflakes (GNFs) with well-defined geometries and accessible electronic properties. Here, we present a simple strategy to fabricate quasi-free-standing GNFs of variable sizes, performing temperature programmed growth of graphene flakes on the Ir(111) surface and subsequent intercalation of gold. Using scanning tunneling microscopy (STM), we show that epitaxial GNFs on a perfectly ordered Au(111) surface are formed while maintaining an unreconstructed, singly hydrogen-terminated edge structure, as confirmed by the accompanying density functional theory (DFT) calculations. Using tip-induced lateral displacement of GNFs, we demonstrate that GNFs on Au(111) are to a large extent decoupled from the Au(111) substrate. The direct accessibility of the electronic states of a single GNF is demonstrated upon analysis of the quasiparticle interference patterns obtained by low-temperature STM. These findings open up an interesting playground for diverse investigations of graphene nanostructures with possible implications for device fabrication.

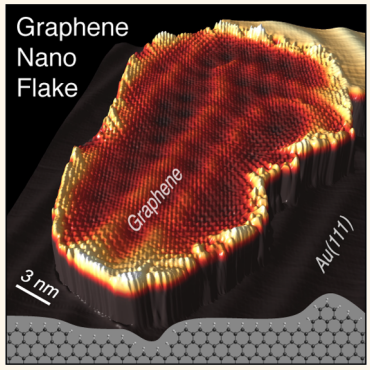

KEYWORDS: graphene nanoflakes · graphene · gold · intercalation · scattering · quasiparticle interference · scanning tunneling microscopy · density functional theory

Graphene nanoribbons (GNRs)[1,2] or graphene quantum dots (GQDs)[3,4] with atomically smooth edges represent one of the most exciting fields of graphene research, because they are predicted to exhibit peculiar electronic and magnetic properties, such as band gaps,[5] localized edge states[5−7] and spin polarization.[8,9] Recently, a number of experiments were reported aiming at the local investigation of the atomic structure and the electronic properties of GQDs. Most commonly, GQDs produced by the high temperature decomposition of organic molecules on metal surfaces, such as Ir(111),[10,11] and Ru(0001)[12] were investigated. In particular, the thermal decomposition of preadsorbed hydrocarbons[11,13] or the unfolding of preadsorbed C_{60} molecules[12] have been incorporated, yielding GQDs with an exceptional structural quality and predominantly zigzag edge configuration. However, the investigation of the local properties of GQDs on Ir(111)[14−18] has left questions open to what extent graphene states prevail compared to substrate contributions and whether the undisturbed electronic states at the edges can be probed in this system. An improved accessibility of the electronic properties of confined graphene structures has recently been reported for GNRs on the Au(111) surface.[2,19−22] Direct observation of the edge states[2] as well as the band gap tuning[20,21] were reported, underlining the accessibility of the electronic properties of graphene nanostructures on Au(111). However, graphene preparation on the chemically inert Cu, Ag and Au surfaces lacks the ease and flexibility of the graphene growth on Ir(111)[10,11,23] or Ru(0001)[24] and requires either the prior design of appropriate precursor molecules[19−21] or amendments to simple hydrocarbon decomposition processes. Very high temperatures in combination with either irradiation by ethylene[25] or atomic carbon deposition[26,27] have been

* Address correspondence to mikhail.fonin@uni-konstanz.de.

Received for review January 21, 2014 and accepted March 25, 2014.

Published online April 02, 2014
10.1021/nn500396c

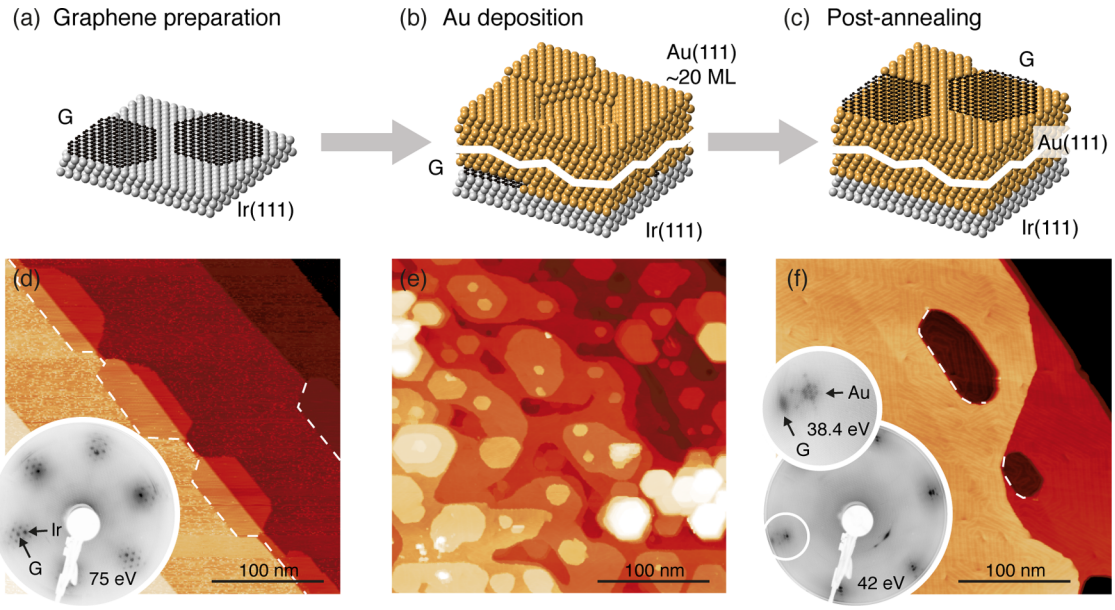

Figure 1. Preparation of graphene flakes on Au(111). (a−c) Schematic representation of the preparation procedure. (d) A topographic STM overview with large GNFs on Ir(111). (e) Sample surface topography after the deposition of nominally 50 Å of Au. (f) STM topography of the sample surface after postannealing. The insets show the evolution of LEED diffraction patterns corresponding to GNFs/Ir(111) and postannealed GNFs/Au/Ir(111). STM images are acquired at room temperature. Tunneling parameters: (d) U_T = 0.5 V, I_T = 1.0 nA, T = 300 K; (e) U_T = 1.0 V, I_T = 0.33 nA, T = 300 K; (f) U_T = 0.21 V, I_T = 0.66 nA; T = 300 K.

shown to form large graphene patches, yet both of the latter approaches fall short in growing small and well-shaped graphene flakes.

RESULTS AND DISCUSSION

Here, we present a simple strategy for the full epitaxial *in situ* preparation of quasi-free-standing GNFs on Au(111) [Figure 1(a−c)] based on the intercalation[28−30] of thick layers of gold. Within the first preparation step, GNFs are formed on the Ir(111) surface by means of high temperature decomposition of room temperature preadsorbed ethylene molecules[11] [Figure 1(d)]. In the second preparation step, the sample is covered by nominally 50−100 Å of gold resulting in an epitaxial Au(111) layer [Figure 1(e)]. Finally, in the third step a postannealing of the sample at 400−500 °C promotes the intercalation of Au and leads to an increase in structural quality of the Au film [Figure 1(f)]. Small depressions within large Au terraces are easily identified as graphene flakes on the Au surface from their shape, suggesting that intact GNFs diffuse from the Au/Ir interface to the top of the Au layer during postannealing [see Supporting Information Figure S1 for further comments on the intercalation process].

Low-energy electron diffraction (LEED) evidences the diffusion of GNFs to the Au surface. Initially, the diffraction pattern of the graphene/Ir(111) system [inset in Figure 1(d)] shows the (1 × 1) spots of graphene and Ir(111) surrounded by the sharp superstructure spots, which correspond to the Moiré structure. After Au deposition and annealing, a specific diffraction pattern is formed, which stems from the Au(111) herringbone reconstruction[31,32] in conjunction with fairly sharp (1 × 1) graphene spots indicative of the presence of GNFs on the Au surface [inset in Figure 1(f)]. LEED shows that graphene flakes appear solely in *R*0 configuration, *i.e.*, with the graphene [1$\bar{1}$00] and the Au [11$\bar{2}$] directions aligned. A slight broadening of the graphene spots is attributed to small angular deviations of the prepared GNFs from an *R*0 alignment.

A direct proof for the presence of graphene flakes on the Au surface is provided from more detailed STM topographies. Figure 2(a) presents a zoom of the largest depression observed in Figure 1(f) and reveals a Moiré structure superposed onto the faintly visible lines of the herringbone reconstruction of the underlying Au(111) substrate. The superposition of Moiré and herringbone reconstruction leads to a complicated superstructure appearance[26,27] confirming the presence of an undisturbed GNF within the depression. GNFs embedded within the topmost Au layer represent the majority of the observed flakes, with the depression depth ranging between 1 and 5 Au(111) atomic layers [Figure 2(b)].

Along with *embedded* GNFs, we also observe GNFs sitting directly on top of the Au(111) surface. In Figure 2(c) the STM topography of such a *floating* GNF is presented. *Floating* GNFs appear either completely isolated on Au(111) terraces or attached to step edges. For all observed floating GNFs, the herringbone reconstruction is unaffected by the presence of the GNF underlining a very weak interaction between graphene and the supporting Au(111) substrate.

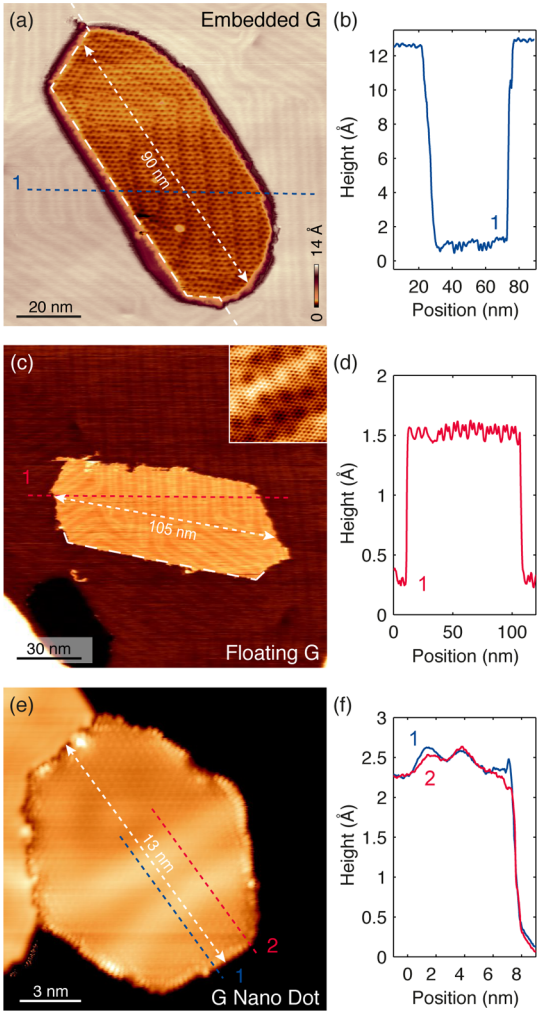

Figure 2. *Embedded* and *floating* graphene flakes on the Au(111) surface. (a) STM topography of an *embedded* GNF on Au(111). (b) Height profile along the line in (a) showing the Moiré structure and the herringbone reconstruction. (c) STM topography of a *floating* GNF including an atomically resolved magnification of the flake in the inset (6×6 nm^2). (d) Height profile along the line shown in (c). (e) STM topography of a small *floating* GNF connected to an Au(111) terrace and the corresponding height profiles (f). Tunneling parameters: (a) $U_T = 0.17$ V, $I_T = 1.85$ nA, $T = 300$ K; (c) $I_T = 0.23$ V, $I_T = 2.0$ nA, $T = 300$ K; (c, inset) $U_T = 0.15$ V, $I_T = 1.7$ nA, $T = 300$ K; (e) $U_T = -50$ mV, $I_T = 1.5$ nA, $T = 6.8$ K.

The size and density of GNFs can be easily tuned by adjusting the preparation parameters, such as temperature and amount of preadsorbed hydrocarbon molecules, during the initial growth on the Ir(111) surface. As an important example we show that very small graphene dots (diameter ~10 nm) of regular shapes and with edges well aligned along graphene zigzag directions could be initially prepared on Ir(111) and successfully decoupled as shown in Figure 2(e). Line profiles across *floating* GNFs in Figure 2(d,f) show completely flat edges suggesting no substantial interaction between the edge and the Au(111) surface, which otherwise would lead to the pronounced corrugation at edges or even to dome-shape structures.[16,33]

High resolution STM topographs give a direct insight into the atomic arrangement of the edges of *floating* GNFs on Au(111) [Figure 3(a,b)]. The flake in Figure 3(a) features a long edge region, which runs mainly parallel to the zigzag direction of graphene with some intermediate armchair segments included [Figure 3(b)]. The appearance of the zigzag regions features bright spots aligned along arcs beginning at the flake edge and then bending into the graphene flake interior [see Figure 3(b)]. In the vicinity of zigzag edges the highest STM intensity is concentrated on one carbon sublattice leading to the observation of single atomic protrusions instead of carbon rings. Further into the flake the intensity of the edge sublattice decays and the honeycomb lattice is completely restored within several nanometers [see inset in Figure 3(a)].

The experimentally observed atomic arrangements of the edges were compared with the results of the DFT calculations for a free-standing graphene sheet with unreconstructed and singly hydrogen terminated edges (one hydrogen atom per edge carbon atom). The simulated STM image of the edge region calculated in the Tersoff–Hamann approximation [Figure 3(c)] shows that for zigzag segments the majority of local density of states (LDOS) is concentrated on the terminating C–H group and the corresponding edge sublattice. The interruption of the zigzag edge segments by armchair or by a combination of short zigzag and armchair segments reduces the LDOS of specific atoms in the bright edge sublattice and commonly leads to the formation of arc-like-features, which decay into the graphene interior as observed in STM images. The details visible in the simulated STM image are overall in very good agreement with the experimentally observed intensity variations within the GNF edge region. Contrarily, the calculations performed for the free-standing graphene flakes with unsaturated and unreconstructed edges lead to completely different results, and consequently the simulations show only poor agreement with the experimental STM data [see Supporting Information Figure S2]. In addition we would like to emphasize that the implemented preparation method allows for the preparation of GNFs with very long zigzag edge segments shown in Figure 3(d) or for the preparation of regular small GNFs almost completely terminated by zigzag edges [Figure 2(e)]. Additionally, edge regions with more complicated atomic structure are also found, depending on the initial growth of the GNFs on Ir(111). An example is magnified in the inset in Figure 3(d) and shows the formation of distinctively different LDOS modulations compared to the long zigzag edge segments. Chevron-type LDOS modulations propagate into the interior of the GNF and are characteristic for rougher edges containing a larger amount of armchair segments.[34,35]

All types of *floating* GNFs show comparable LDOS features for similar edge composition; therefore, we conclude that flakes prepared in that way become

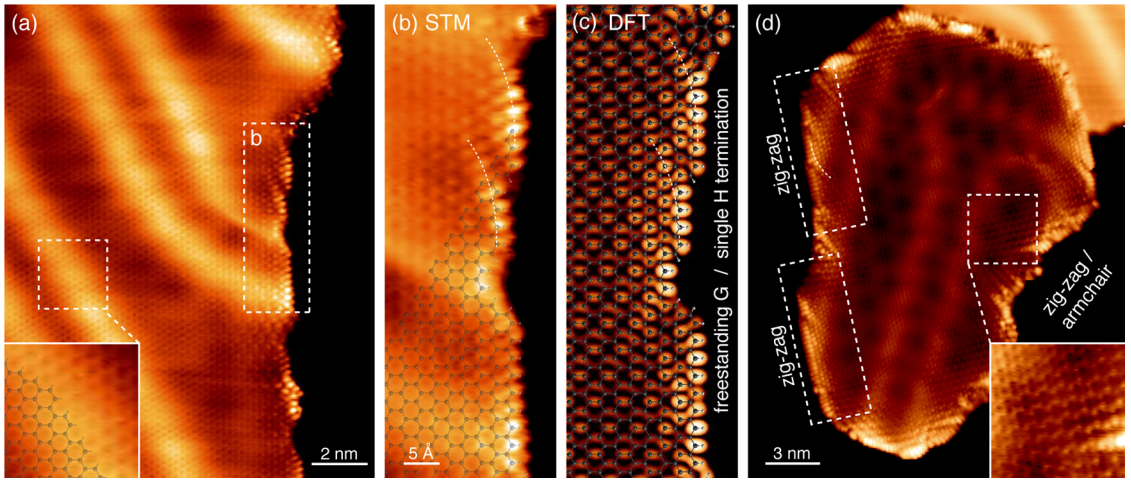

Figure 3. Atomic structure of the edges of graphene flakes on Au(111). (a) Atomically resolved STM topography of an edge region of a GNF. The inset shows the carbon rings within the flake. (b) Magnification of the area marked in (a). (c) Simulated STM image of a freestanding graphene segment reproducing the experimental geometry ($E - E_F = 0...-0.3$ eV). The graphene honeycomb lattice is superposed. (d) Atomically resolved STM topography showing a small GNF on Au(111). Tunneling parameters: (a,b) $U_T = -0.3$ V, $I_T = 1.2$ nA, $T = 10$ K; (d) $U_T = 0.3$ V, $I_T = 1.0$ nA; $T = 10$ K.

hydrogen terminated during the preparation. Furthermore we find that the LDOS of various edge configurations as well as the corresponding propagation of LDOS modulations into the flake interior is consistent with the patterns observed for the edge structures of hydrogen terminated highly oriented pyrolithic graphite[35,36] as well as with recently studied hydrogenated GNRs on Au.[37] This fact hints at negligible interaction of H-terminated graphene edges with the Au surface, a finding previously predicted from DFT calculations for singly H-terminated graphene nanoribbons on Au(111) surfaces.[38] In the latter work, localized states at zigzag graphene edges were shown to survive in the case of GNR/Au(111), consistent with our STM images showing considerable enhancement of the intensity at the edge atoms of zigzag regions [Figure 2(e) and Figure 3(b,d)].

The hydrogen termination of the edges of GNFs together with the overall weak interaction of graphene with the Au surface[25−27] are impressively supported by the fact that *floating* graphene flakes, which are not connected to step edges can be displaced by the STM tip with only moderate tunneling currents. A sequence of STM topographies in Figure 4 illustrates the lateral displacement of a *floating* GNF at room temperature. The flake extends over two Au terraces and is initially found in the *R*0 configuration. During scanning, the flake is pushed up a gold terrace and simultaneously rotated. Subsequent scanning reveals its new position and angular orientation [Figure 4(b)]. In the course of the experiment the flake is repeatedly displaced on top of the terrace and rotated compared to the initial *R*0 configuration as shown in Figure 4(c). Tunneling parameters for the displacement were typically in the 1 nA range for tunnel voltages of 1 V. We found that it is possible to move large flakes (Figure 4) as well as

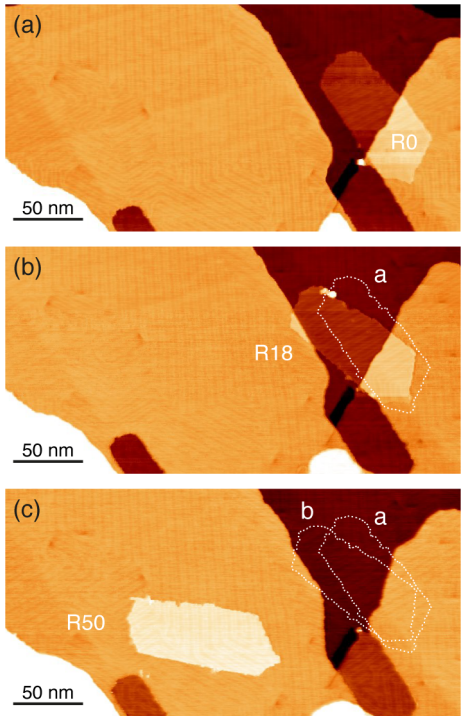

Figure 4. Lateral manipulation of a *floating* graphene flake on Au(111). (a−c) Sequence of STM images showing the tip induced lateral displacement of a *floating* GNF with the size of approximately 105 × 40 nm^2. (a) The flake is initially found in *R*0 orientation, (b) rotated by about 18° during scanning, and (c) pushed up the terrace and further rotated to 50° compared to *R*0. Tunneling parameters: (a) $U_T = 1.0$ V, $I_T = 0.3$ nA; (b) $U_T = 1.0$ V, $I_T = 0.55$ nA; (c) $U_T = 0.23$ V, $I_T = 2.0$ nA. All images acquired at $T = 300$ K.

smaller flakes [<40 × 40 nm^2, see Supporting Information Figure S3] if the flakes are *floating* and not pinned by Au clusters occasionally present on the surface. The experiments on the lateral manipulation of large graphene flakes on the Au(111) surface suggests the

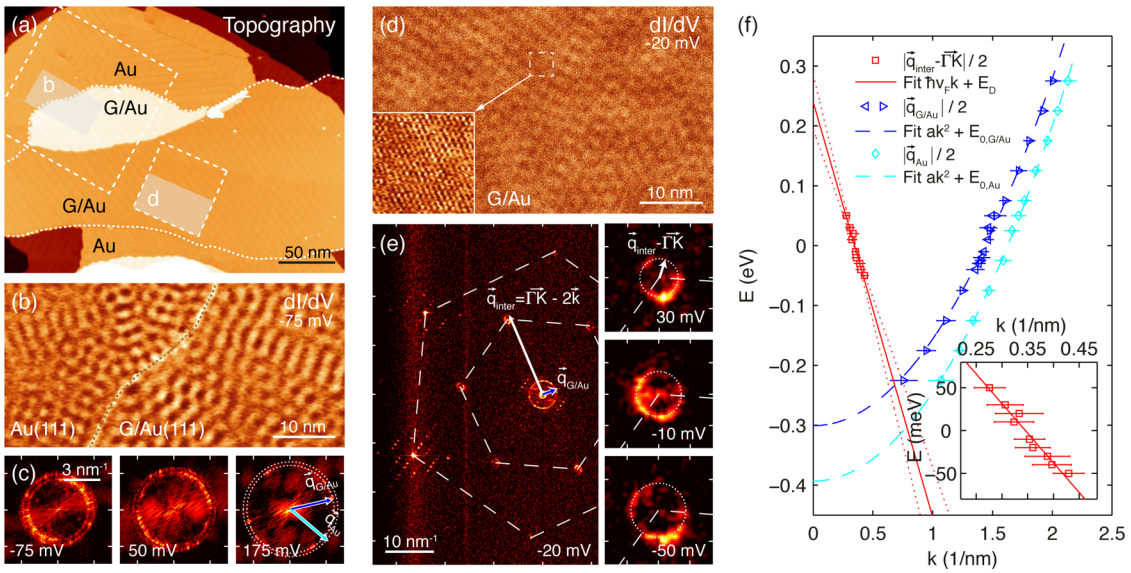

Figure 5. Electronic structure of graphene/Au(111). (a) Topography of an approximately 400 × 160 nm^2 large flake used for d*I*/d*V* mappings. (b) d*I*/d*V* map across the rim of a large graphene flake showing the quasiparticle interferences of the Au surface state. Tunneling parameters: $U_T = -75$ mV, $I_T = 1$ nA, $T = 8$ K. (c) Fast Fourier transform of a 109 × 109 nm^2 large area partially depicted in (b) at selected bias voltages. (d) d*I*/d*V* map on the graphene flake with atomic resolution. Tunneling parameters: $U_T = -20$ mV, $I_T = 1$ nA, $T = 7.7$ K. (e) Fast Fourier transform of a 54 × 54 nm^2 map partially depicted in (d) showing a rich structure including atomic, Moiré, and herringbone features as well as *intervalley* scattering features. The right column shows magnifications of the *intervalley* scattering rings (3.5 × 3.5 nm^{-2}) at different bias voltages. (f) The Au(111) surface state dispersion for pristine Au(111) (cyan diamonds) as well as for graphene/Au(111) (blue triangles). Dispersion relation of the graphene electrons determined from the intervalley scattering (red squares) and corresponding fit (red line) including uncertainty (red dotted lines) determined from a series of atomically resolved constant-energy mappings. The *k* values are plotted with respect to the Γ-point in the case of the surface state and with respect to the K-point in case of graphene.

energy barrier for displacement of graphene on Au to be of the same magnitude as for a second layer of graphene on top of the graphene/Ru(0001) system,[39] thus underlining graphene/Au(111) to be an exceptional system because of the lack of decisive graphene–substrate interactions compared to many other metal surfaces commonly used.[18,33,40]

The weak interaction between graphene and the underlying metal substrate is expected to be a crucial prerequisite for the local investigation of the electronic properties of graphene. Here we analyze the quasiparticle interference patterns in single graphene flakes, which give a direct access to the band structure of graphene.[41−43] All measurements presented here were performed on one single *R*0 GNF approximately 400 nm long and 160 nm wide as well as on the Au(111) surface in proximity to the flake [see Figure 5(a)]. The edges of the flake were only partly free-standing, which assured no tip-induced GNF displacements also at higher tunneling currents. We first focus on the modulations of LDOS that are associated with the elastic impurity scattering of the surface state electrons of Au(111). For this purpose we acquire d*I*/d*V* maps across the rim of the graphene flake in an area of 109 × 109 nm^2 in the top left corner of Figure 5(a). A constant-energy map obtained at −75 meV is partially depicted in Figure 5(b) showing spatial LDOS modulations, which are clearly visible both on the pure Au(111) surface (left side) and within the GNF interior (right side). [The full mapping can be found in Supporting Information Figure S4.]

In order to extract the scattering vectors $\vec{q}$ characteristic for the observed interference patterns, fast Fourier transforms (FFT) of d*I*/d*V* maps were used. The corresponding FFTs are depicted in Figure 5(c) and display two distinct circles centered at $\vec{q} = 0$. Selective area FFTs show that the outer circle originates from the bare Au(111) surface areas, whereas the inner circle is due to the graphene covered Au(111) surface. The sharp ring is characteristic for the backscattering process within the ring-like constant energy contour of the parabolic Au(111) surface state centered at the Γ-point.[44] The measured radius q_{Au} is connected to the momentum of a scattered electron *via* $q_{Au} = 2k$ for backscattered electrons, and since d*I*/d*V* maps selectively probe electrons of energy corresponding to the applied tip voltage, one can directly plot the dispersion relation $E(k)$ [cyan diamonds and line in Figure 5(f)]. The parabolic dispersion on Au(111) with the minimum at $E_{0,Au} = (-0.39 \pm 0.02)$ eV and the effective mass of $m^*_{Au} = (0.26 \pm 0.03)m_e$ clearly identifies the corresponding electronic states as the Shockley surface state of Au(111).[44] The observed energy shift for the position of the surface state compared to the value of −505 meV for Au(111) single crystals[45] is attributed to the Au(111) film thickness and is subject to slight variations across the sample. The dispersion relation extracted from the inner ring feature corresponding to

the graphene covered Au(111) region also shows a parabolic dispersion relation with a clear shift toward lower binding energy [$E_{0,G/Au}$ = (−0.30 ± 0.03) eV; $m^*_{G/Au}$ = (0.26 ± 0.02)m_e]. This shift arises from the presence of the weakly interacting graphene layer, an effect previously observed for noble gases adsorbed on the Au(111) surface.[46] Thus, the observed modulations of LDOS in Figure 5 (b) measured within the graphene flake are solely due to the surface state of the Au(111) substrate, which impressively supports the explanation proposed earlier for graphene flakes on Ir(111).[17]

We now analyze the atomically resolved d*I*/d*V* maps with real space dimensions of 54 × 54 nm^2 and their FFTs obtained on the same GNF [Figure 5(d,e) and Supporting Information Figure S4]. In addition to the circular feature of the Au surface state electrons centered at $\vec{q}$ = 0 [blue arrow in Figure 5(e)], the obtained FFTs show several additional features. First of all, six outermost spots corresponding to the atomic structure of graphene are visible in Figure 5(e), which are superposed by the spots originating form the herringbone reconstruction of Au(111) and the Moiré structure of graphene. Most importantly, we observe small ring-like features constituting a hexagon rotated by 30° as compared to the first order atomic spots. These features were previously shown to stem from the *intervalley* scattering, which produces the ($\sqrt{3}$ × $\sqrt{3}$)*R*30° superstructure in the real space images.[41−43]

For the *intervalley* scattering, the corresponding scattering vectors $\vec{q}_{\text{inter}}$ connect the states with antiparallel $\vec{k}$ and $\vec{k'}$ at the constant-energy circles of two adjacent points K and K′ at the corners of the graphene Brillouin zone, where the vectors $\vec{k}$ and $\vec{k'}$ have their origins in the K and K′ points, respectively. Thus for the scattering vectors we can write $\vec{q}_{\text{inter}} = \vec{\Gamma K} - 2\vec{k}$. Taking into account all possible directions of $\vec{k}$ for all high symmetry points K and K′, we obtain six circles with radius $|\vec{q}_{\text{inter}} - \vec{\Gamma K}| = 2k$ in the FFT at a given bias voltage used for the determination of the dispersion relation *E*(*k*). Figure 5(f) (red squares) shows *E*(*k*) for the energy range between −50 meV and +50 meV. The *k* values of graphene are plotted with respect to the K-point. The dispersion relation for the investigated graphene flake is found to be linear, and a fit with $E(k) = \hbar v_F k + E_D$ yields an estimation of the Fermi velocity of $v_F = (1.1 \pm 0.2) \cdot 10^6$ m/s and a Dirac point positioned at E_D = (+0.24 ± 0.05) eV. In agreement with the previous photoemission studies[26,47,48] our graphene flakes are *p*-doped; however, our quantitative value for the Dirac point slightly exceeds the value of 100−150 meV[47,48] reported for the monolayer graphene/gold systems. The shift in the position of the Dirac point could possibly be accounted to the influence of the electrostatic potential of the tip.[49,50] The simultaneous experimental observation of the scattering features attributed to the Au(111) surface state electrons and to the *intervalley* scattering of graphene electrons offers a possibility to distinguish between the two electronic systems in the studied energy range, which has been a matter of discussion in previous experiments on graphene/metal systems.[14−17]

CONCLUSION

We have demonstrated that quasi-free-standing GNFs on the Au(111) surface can be obtained by an intercalation-based all-epitaxial preparation. The proposed method yields very good results for the controlled preparation of GNFs with sizes ranging from several nanometers to a few hundred nanometers. Moreover, this method offers the flexibility to exchange Au as an intercalant by other metals, such as Ag or Cu,[28] in order to tailor the graphene doping level and to exploit alternative graphene growth techniques[12] or other metal substrates for growth of GNFs of desired size, shape and edge termination. Our STM results combined with the DFT calculations show that the prepared GNFs have atomically well-defined edges, which are unaffected by the proximity of the Au(111) substrate and are naturally terminated by hydrogen, thus giving a playground for further local investigations of the electronic and possibly magnetic properties of the edges. We observe only very weak coupling of the prepared GNFs to the substrate as confirmed by lateral displacement of the flakes with the STM tip, which might allow to fabricate confined multilayer graphene structures or coupled graphene quantum dots. The presented dispersion relation of one single graphene flake unambiguously shows that the electronic structure of GNFs on Au(111) can be accessed separately from those of the underlying Au(111) substrate, which is of paramount importance for further local investigations of the electronic properties of confined graphene structures.

METHODS

Experimental Setup. The presented measurements were prepared in two ultrahigh vacuum (UHV) systems (base pressure 5 × 10^{-11} mbar). Room temperature STM experiments were carried out using an Omicron variable temperature STM, whereas an Omicron Cryogenic STM was used for the low temperature measurements (6−12 K). All STM measurements were performed in the constant-current-mode using electrochemically etched polycrystalline tungsten tips cleaned in UHV by flash-annealing. The sign of the bias voltage corresponds to the potential applied to the sample. Tunneling current and voltage are given in the figure caption. d*I*/d*V* mappings were performed at low temperatures using the lock-in-technique with modulation voltage between 2 and 4 mV RMS and modulation frequency of 664.7 Hz. Tunneling current for d*I*/d*V* mappings was between 800 pA and 2 nA. d*I*/d*V* mappings of the Au surface state were recorded using 512 × 512 pixels^2 and 120 × 120 nm^2, atomically resolved d*I*/d*V* mappings were recorded with 1024 × 1024 pixels^2 and 60 × 60 nm^2 and

subsequently calibrated to the graphene lattice with $a_G = 2.46$ Å. The values for the q-vectors were obtained from the radial distribution of intensity after an azimuthal integration around the center of the rings in the FFTs. Crystallographic illustrations are generated using CrystalMaker, CrystalMaker Software, Ltd., England.

Sample Preparation. Before every experiment, the Ir(111) crystal (MaTecK GmbH) was cleaned by several cycles of Ar^+ sputtering (2 kV), oxygen annealing (900−1150 °C, 5×10^{-7} mbar O_2 pressure) and flash annealing (5 s up to 1800 °C). The cleanliness of the Ir(111) crystal was checked by LEED and STM. Graphene was prepared by 1−2 subsequent temperature programmed growth (TPG) cycles. For each TPG cycle the Ir(111) surface was exposed to an ethylene dose between 2 and 7 Langmuir at room temperature and subsequently annealed for 25 s with the temperature held between $T_{t=0s} = 1100$ and $T_{t=25s} = 1300$ °C for large flakes and $T_{t=0s} = 930$ and $T_{t=25s} = 1220$ °C for small flakes. Deviations from this preparation procedure are explicitly mentioned in the manuscript text. Gold was evaporated from an effusion cell. The sample was at room temperature during gold deposition. Subsequently, the sample was annealed to desired temperatures.

Theoretical Support. DFT calculations were carried out using the projector augmented plane wave method,[51] a plane wave basis set with a maximum kinetic energy of 500 eV and the PBE exchange-correlation potential,[52] as implemented in the VASP program.[53] The surface Brillouin zone is sampled with a 3 × 3 k-point mesh centered at the Gamma point. The slab replicas are separated by *ca.* 15 Å in the surface normal direction. C−C and C−H bond lengths were set to 1.442 and 1.084 Å, respectively, and no further structural relaxation was performed. The STM images are calculated using the Tersoff−Hamann formalism[54] as implemented in the HIVE visualization software.[55]

Conflict of Interest: The authors declare no competing financial interest.

Acknowledgment. This work has been supported by the European Science Foundation under the EUROCORES Programme EuroGRAPHENE (Project SpinGraph) and by the Deutsche Forschungsgemeinschaft within the Priority Program (SPP) 1459. M.F. gratefully acknowledges the financial support by the Research Center UltraQuantum (Excellence Initiative). Computer time at the North-German Supercomputing Alliance (HLRN) is greatfully acknowledged.

Supporting Information Available: Figure S1: Additional information on the intercalation process. Figure S2: DFT calculations of graphene edges. Figure S3: Additional example of lateral displacement of GNFs. Figure S4: STM topographies and constant energy mappings for the analysis of dispersion relations. Figure S5: Magnifications of the intervalley scattering discs at various energies and corresponding radial distribution of intensity. This material is available free of charge *via* the Internet at http://pubs.acs.org.

REFERENCES AND NOTES

1. Son, Y.-W.; Cohen, M. L.; Louie, S. G. Half-Metallic Graphene Nanoribbons. *Nature* **2006**, *444*, 347–349.
2. Tao, C.; Jiao, L.; Yazyev, O. V.; Chen, Y.-C.; Feng, J.; Zhang, X.; Capaz, R. B.; Tour, J. M.; Zettl, A.; Louie, S. G.; *et al.* Spatially Resolving Edge States of Chiral Graphene Nanoribbons. *Nat. Phys.* **2011**, *7*, 616–620.
3. Ponomarenko, L. A.; Schedin, F.; Katsnelson, M. I.; Yang, R.; Hill, E. W.; Novoselov, K. S.; Geim, A. K. Chaotic Dirac Billiard in Graphene Quantum Dots. *Science* **2008**, *320*, 356–358.
4. Ritter, K. A.; Lyding, J. W. The Influence of Edge Structure on the Electronic Properties of Graphene Quantum Dots and Nanoribbons. *Nat. Mater.* **2009**, *8*, 235–242.
5. Brey, L.; Fertig, H. Electronic States of Graphene Nanoribbons Studied with the Dirac Equation. *Phys. Rev. B: Condens. Matter Mater. Phys.* **2006**, *73*, 235411.
6. Nakada, K.; Fujita, M.; Dresselhaus, G.; Dresselhaus, M. Edge State in Graphene Ribbons: Nanometer Size Effect and Edge Shape Dependence. *Phys. Rev. B: Condens. Matter Mater. Phys.* **1996**, *54*, 17954.
7. Fujita, M.; Wakabayashi, K.; Nakada, K.; Kusakabe, K. Peculiar Localized State at Zigzag Graphite Edge. *J. Phys. Soc. Jpn.* **1996**, *65*, 1920–1923.
8. Yazyev, O. V. Emergence of Magnetism in Graphene Materials and Nanostructures. *Rep. Prog. Phys.* **2010**, *73*, 056501.
9. Wang, W. L.; Meng, S.; Kaxiras, E. Graphene NanoFlakes with Large Spin. *Nano Lett.* **2008**, *8*, 241–245.
10. N'Diaye, A. T.; Coraux, J.; Plasa, T. N.; Busse, C.; Michely, T. Structure of Epitaxial Graphene on Ir(111). *New J. Phys.* **2008**, *10*, 043033.
11. Coraux, J.; N'Diaye, A. T.; Engler, M.; Busse, C.; Wall, D.; Buckanie, N.; zu Heringdorf, F.-J. M.; van Gastel, R.; Poelsema, B.; Michely, T. Growth of Graphene on Ir(111). *New J. Phys.* **2009**, *11*, 023006.
12. Lu, J.; Yeo, P. S. E.; Gan, C. K.; Wu, P.; Loh, K. P. Transforming C_{60} Molecules into Graphene Quantum Dots. *Nat. Nanotechnol.* **2011**, *6*, 247–252.
13. Olle, M.; Ceballos, G.; Serrate, D.; Gambardella, P. Yield and Shape Selection of Graphene Nanoislands Grown on Ni(111). *Nano Lett.* **2012**, *12*, 4431–4436.
14. Phark, S.-h.; Borme, J.; Vanegas, A. L.; Corbetta, M.; Sander, D.; Kirschner, J. Direct Observation of Electron Confinement in Epitaxial Graphene Nanoislands. *ACS Nano* **2011**, *5*, 8162–8166.
15. Hämäläinen, S. K.; Sun, Z.; Boneschanscher, M. P.; Uppstu, A.; Ijäs, M.; Harju, A.; Vanmaekelbergh, D.; Liljeroth, P. Quantum-Confined Electronic States in Atomically Well-Defined Graphene Nanostructures. *Phys. Rev. Lett.* **2011**, *107*, 236803.
16. Subramaniam, D.; Libisch, F.; Li, Y.; Pauly, C.; Geringer, V.; Reiter, R.; Mashoff, T.; Liebmann, M.; Burgdörfer, J.; Busse, C.; *et al.* Wave-Function Mapping of Graphene Quantum Dots with Soft Confinement. *Phys. Rev. Lett.* **2012**, *108*, 046801.
17. Altenburg, S. J.; Kröger, J.; Wehling, T. O.; Sachs, B.; Lichtenstein, A. I.; Berndt, R. Local Gating of an Ir(111) Surface Resonance by Graphene Islands. *Phys. Rev. Lett.* **2012**, *108*, 206805.
18. Li, Y.; Subramaniam, D.; Atodiresei, N.; Lazić, P.; Caciuc, V.; Pauly, C.; Georgi, A.; Busse, C.; Liebmann, M.; Blügel, S.; *et al.* Absence of Edge States in Covalently Bonded Zigzag Edges of Graphene on Ir(111). *Adv. Mater.* **2013**, *25*, 1967–1972.
19. Cai, J.; Ruffieux, P.; Jaafar, R.; Bieri, M.; Braun, T.; Blankenburg, S.; Muoth, M.; Seitsonen, A. P.; Saleh, M.; Feng, X.; *et al.* Atomically Precise Bottom-Up Fabrication of Graphene Nanoribbons. *Nature* **2010**, *466*, 470–473.
20. Ruffieux, P.; Cai, J.; Plumb, N. C.; Patthey, L.; Prezzi, D.; Ferretti, A.; Molinari, E.; Feng, X.; Müllen, K.; Pignedoli, C. A.; *et al.* Electronic Structure of Atomically Precise Graphene Nanoribbons. *ACS Nano* **2012**, *6*, 6930–6935.
21. Chen, Y.-C.; de Oteyza, D. G.; Pedramrazi, Z.; Chen, C.; Fischer, F. R.; Crommie, M. F. Tuning the Band Gap of Graphene Nanoribbons Synthesized from Molecular Precursors. *ACS Nano* **2013**, *7*, 6123–6128.
22. Van der Lit, J.; Boneschanscher, M. P.; Vanmaekelbergh, D.; Ijäs, M.; Uppstu, A.; Ervasti, M.; Harju, A.; Liljeroth, P.; Swart, I. Suppression of Electron-Vibron Coupling in Graphene Nanoribbons Contacted *via* a Single Atom. *Nat. Commun.* **2013**, *4*, 2023.
23. Voloshina, E. N.; Fertitta, E.; Garhofer, A.; Mittendorfer, M.; Fonin, M.; Thissen, A.; Dedkov, Yu. S. Electronic Structure and Imaging Contrast of Graphene Moiré on Metals. *Sci. Rep.* **2013**, *3*, 1072.
24. Loginova, E.; Bartelt, N. C.; Feibelman, P. J.; McCarty, K. F. Factors Influencing Graphene Growth on Metal Surfaces. *New J. Phys.* **2009**, *11*, 063046.
25. Martínez-Galera, A. J.; Brihuega, I.; Gómez-Rodríguez, J. M. Ethylene Irradiation: A New Route to Grow Graphene on Low Reactivity Metals. *ACS Nano* **2011**, *11*, 3576–3580.
26. Wofford, J. M.; Starodub, E.; Walter, A. L.; Nie, S.; Bostwick, A.; Bartelt, N. C.; Thürmer, K.; Rotenberg, E.; McCarty, K. F.; Dubon, O. D. Extraordinary Epitaxial Alignment of Graphene Islands on Au(111). *New J. Phys.* **2012**, *14*, 053008.

27. Nie, S.; Bartelt, N. C.; Wofford, J. M.; Dubon, O. D.; McCarty, K. F.; Thürmer, K. Scanning Tunneling Microscopy Study of Graphene on Au(111): Growth Mechanisms and Substrate Interactions. *New J. Phys.* **2012**, *85*, 205406.
28. Dedkov, Y.; Shikin, A.; Adamchuk, V.; Molodtsov, S.; Laubschat, C.; Bauer, A.; Kaindl, G. Intercalation of Copper Underneath a Monolayer of Graphite on Ni(111). *Phys. Rev. B: Condens. Matter Mater. Phys.* **2001**, *64*, 035405.
29. Varykhalov, A.; Sánchez-Barriga, J.; Shikin, A.; Biswas, C.; Vescovo, E.; Rybkin, A.; Marchenko, D.; Rader, O. Electronic and Magnetic Properties of Quasifreestanding Graphene on Ni. *Phys. Rev. Lett.* **2008**, *101*, 157601.
30. Petrović, M.; Šrut Rakić, I.; Runte, S.; Busse, C.; Sadowski, J. T.; Lazić, P.; Pletikosić, I.; Pan, Z.-H.; Milun, M.; Pervan, P.; *et al.* The Mechanism of Caesium Intercalation of Graphene. *Nat. Commun.* **2013**, *4*, 2772.
31. van Hove, M. A.; Koestner, R. J.; Stair, P. C.; Bibérian, J. P.; Kesmodel, L. L.; Bartos, I.; Somorjai, G. A. The Surface Reconstructions of the (100) Crystal Faces of Iridium, Platinum and Gold. *Surf. Sci.* **1981**, *103*, 189–217.
32. Harten, U.; Lahee, A.; Toennies, J.; Wöll, Ch. Observation of a Soliton Reconstruction of Au(111) by High-Resolution Helium-Atom Diffraction. *Phys. Rev. Lett.* **1985**, *54*, 2619–2622.
33. Lacovig, P.; Pozzo, M.; Alfè, D.; Vilmercati, P.; Baraldi, A.; Lizzit, S. Growth of Dome-Shaped Carbon Nanoislands on Ir(111): The Intermediate between Carbidic Clusters and Quasi-Free-Standing Graphene. *Phys. Rev. Lett.* **2009**, *103*, 166101.
34. Yang, H.; Mayne, A. J.; Boucherit, M.; Comtet, G.; Dujardin, G.; Kuk, Y. Quantum Interference Channeling at Graphene Edges. *Nano Lett.* **2010**, *10*, 943–947.
35. Kobayashi, Y.; Fukui, K.; Enoki, T.; Kusakabe, K.; Kaburagi, Y. Observation of Zigzag and Armchair Edges of Graphite Using Scanning Tunneling Microscopy and Spectroscopy. *Phys. Rev. B: Condens. Matter Mater. Phys.* **2005**, *71*, 193406.
36. Kobayashi, Y.; Fukui, K.; Enoki, T. Edge State on Hydrogen-Terminated Graphite Edges Investigated by Scanning Tunneling Microscopy. *Phys. Rev. B: Condens. Matter Mater. Phys.* **2006**, *73*, 125415.
37. Zhang, X.; Yazyev, O. V.; Feng, J.; Xie, L.; Tao, C.; Chen, Y.-C.; Jiao, L.; Pedramrazi, Z.; Zettl, A.; Louie, S. G.; *et al.* Experimentally Engineering the Edge Termination of Graphene Nanoribbons. *ACS Nano* **2013**, *7*, 198–202.
38. Li, Y.; Zhang, W.; Morgenstern, M.; Mazzarello, R. Electronic and Magnetic Properties of Zigzag Graphene Nanoribbons on the (111) Surface of Cu, Ag, and Au. *Phys. Rev. Lett.* **2013**, *110*, 216804.
39. Feng, X.; Kwon, S.; Park, J. Y.; Salmeron, M. Superlubric Sliding of Graphene Nanoflakes on Graphene. *ACS Nano* **2013**, *7*, 1718–1724.
40. Ugeda, M.; Fernández-Torre, D.; Brihuega, I.; Pou, P.; Martínez-Galera, A.; Pérez, R.; Gómez-Rodríguez, J. Point Defects on Graphene on Metals. *Phys. Rev. Lett.* **2011**, *107*, 116803.
41. Rutter, G. M.; Crain, J. N.; Guisinger, N. P.; Li, T.; First, P. N.; Stroscio, J. A. Scattering and Interference in Epitaxial Graphene. *Science* **2007**, *317*, 219–222.
42. Simon, L.; Bena, C.; Vonau, F.; Cranney, M.; Aubel, D. Fourier-Transform Scanning Tunnelling Spectroscopy: The Possibility To Obtain Constant-Energy Maps and Band Dispersion Using a Local Measurement. *J. Phys. D: Appl. Phys.* **2011**, *44*, 464010.
43. Mallet, P.; Brihuega, I.; Bose, S.; Ugeda, M.; Gómez-Rodríguez, J.; Kern, K.; Veuillen, J. Role of Pseudospin in Quasiparticle Interferences in Epitaxial Graphene Probed by High-Resolution Scanning Tunneling Microscopy. *Phys. Rev. B: Condens. Matter Mater. Phys.* **2012**, *86*, 045444.
44. Crommie, M. F.; Lutz, C. P.; Eigler, D. M. Imaging Standing Waves in a Two-Dimensional Electron Gas. *Nature* **1993**, *363*, 524–527.
45. Kliewer, J.; Berndt, R.; Chulkov, E. V.; Silkin, V. M.; Echenique, P. M.; Crampin, S. Dimensionality Effects in the Lifetime of Surface States. *Science* **2000**, *288*, 1399–1402.
46. Andreev, T.; Barke, I.; Hövel, H. Adsorbed Rare-Gas Layers on Au(111): Shift of the Shockley Surface State Studied with Ultraviolet Photoelectron Spectroscopy and Scanning Tunneling Spectroscopy. *Phys. Rev. B: Condens. Matter Mater. Phys.* **2004**, *70*, 205426.
47. Marchenko, D.; Varykhalov, A.; Rybkin, A.; Shikin, A. M.; Rader, O. Atmospheric Stability and Doping Protection of Noble-Metal Intercalated Graphene on Ni(111). *Appl. Phys. Lett.* **2011**, *98*, 122111.
48. Enderlein, C.; Kim, Y. S.; Bostwick, A.; Rotenberg, E.; Horn, K. The Formation of an Energy Gap in Graphene on Ruthenium by Controlling the Interface. *New J. Phys.* **2010**, *12*, 033014.
49. Min, H.; Adam, S.; Song, Y. J.; Stroscio, J. A.; Stiles, M. D.; MacDonald, A. H. Landau Levels and Band Bending In Few-Layer Epitaxial Graphene. *Phys. Rev. B: Condens. Matter Mater. Phys.* **2011**, *83*, 155430.
50. Brar, V. W.; Decker, R.; Solowan, H.-M.; Wang, Y.; Maserati, L.; Chan, K. T.; Lee, H.; Girit, C. O.; Zettl, A.; Louie, S. G.; *et al.* Gate-Controlled Ionization and Screening of Cobalt Adatoms on a Graphene Surface. *Nat. Phys.* **2010**, *7*, 43–47.
51. Blöchl, P. Projector Augmented-Wave Method. *Phys. Rev. B: Condens. Matter Mater. Phys.* **1994**, *50*, 17953.
52. Perdew, J.; Burke, K.; Ernzerhof, M. Generalized Gradient Approximation Made Simple. *Phys. Rev. Lett.* **1996**, *77*, 3865.
53. Kresse, G.; Hafner, J. Norm-Conserving and Ultrasoft Pseudopotentials for First-Row and Transition Elements. *J. Phys.: Condens. Matter* **1994**, *6*, 8245.
54. Tersoff, J.; Hamann, D. Theory of the Scanning Tunneling Microscope. *Phys. Rev. B: Condens. Matter Mater. Phys.* **1985**, *31*, 805–813.
55. Vanpoucke, D. E. P.; Brocks, G. Formation of Pt-Induced Ge Atomic Nanowires on Pt/Ge(001): A Density Functional Theory Study. *Phys. Rev. B: Condens. Matter Mater. Phys.* **2008**, *77*, 241308.